



SUPPLEMENTARY MATERIAL TO  
**Quantitative structure–activity relationship modelling of influenza  
M2 ion channels inhibitors**

IVANKA G. STANKOVA<sup>1\*</sup>, RADOSLAV L. CHAYROV<sup>1</sup>, MICHAELA SCHMIDTKE<sup>2</sup>,  
DANCHO L. DANALEV<sup>3\*\*</sup>, LIUDMILA N. OGNICHENKO<sup>4</sup>, ANATOLY G.  
ARTEMENKO<sup>4</sup>, VALERY A. SHAPKIN<sup>5</sup> and VICTOR E. KUZ'MIN<sup>4</sup>

<sup>1</sup>Department of Chemistry, South-West University “Neofit Rilski”, Blagoevgrad, 2700, Bulgaria, <sup>2</sup>Friedrich Schiller University, Department of Virology and Antiviral Therapy, Jena, 207745, Germany, <sup>3</sup>University of Chemical Technology and Metallurgy, Biotechnology Department, 1756 Sofia, 8 blvd. Kliment Ohridski, Bulgaria, <sup>4</sup>A.V. Bogatsky Physico-Chemical Institute of Ukrainian National Academy of Sciences, Department of Molecular Structure and Chemoinformatics, 86, Lustdorfskaya doroga, Odessa, 65080, Ukraine and

<sup>5</sup>Department of Theoretical Foundations of Chemistry, Odessa National Polytechnic University, 1, Shevchenko ave., Odessa 65044, Ukraine

J. Serb. Chem. Soc. 86 (7–8) (2021) 625–637

Fig. S-1 depicts the example showing how, using vertexes differentiation by atomic charges, the simplexes descriptors are generated at 2D level.

The contribution of each of nine SiRMS descriptors used in the Model A1 is represented in Table S-I.

The distribution of prediction errors ( $\Delta Y = \text{mod}(Y_{\text{predicted}} - Y_{\text{observed}})$ ) demonstrates that a greater accuracy of prediction is observed for compounds with medium (Fig. S-3).

\* \*\* Corresponding authors. E-mail: (\*)ivastankova@abv.bg; (\*\*)ddanalev@uctm.edu

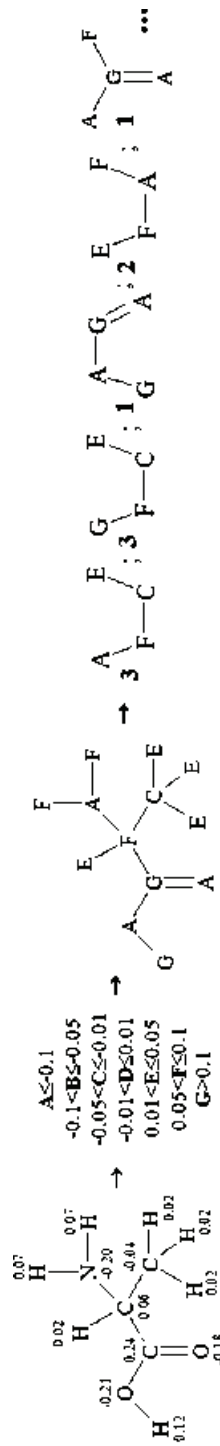


Fig. S-1. Depiction of the development of simplex descriptors at 2D level.

TABLE S-1. Structural parameters and their VIP scores

No.	Type differentiation vertexes simplexes	Structural fragment	VIP scores
	Atom charge	A—F---D	0.78
1		$\begin{array}{c} \bullet \\ C \end{array}$	
2	Type	$\begin{array}{c} & & \bullet \\ & \diagup & \diagdown \\ \diagup & C & \diagdown \\ H & & \end{array}$	0.45
	Atom charge	A=G—E	0.44
3		$\begin{array}{c} \bullet \\ F \end{array}$	
4	lipophilicity	$\begin{array}{c} D & D \\ \diagup & \diagdown \\ D & G \end{array}$	0.41
5	type	$\begin{array}{c} N \\    \\ C & C \\ \diagup & \diagdown \end{array}$	0.41
6	lipophilicity	$\begin{array}{c} D & E \\ G & \diagup \diagdown \\ D & D \end{array}$	0.39
7	lipophilicity	D—C	0.33
8	Atom charge	$\begin{array}{c} C \\   \\ C-D-D \end{array}$	0.30
9	lipophilicity	E—D—G	0.23
		$\begin{array}{c} \bullet \\ C \end{array}$	

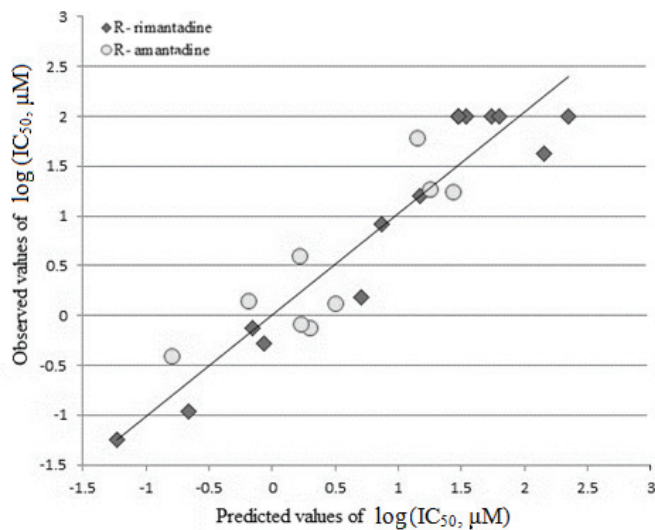


Fig. S-2. Observed vs. predicted diagram of antiviral activity ( $\log IC_{50}$ ) for 22 molecules (Model A1).

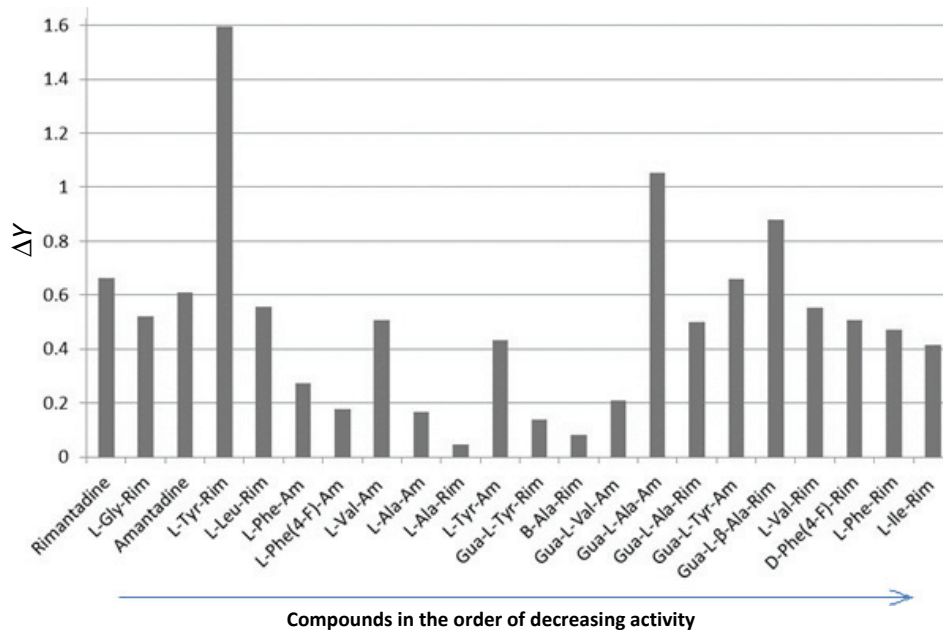


Fig. S-3. The distribution of activity prediction errors ( $\Delta Y$ ) by Model A2.

TABLE S-II. Predicted classes of activity by models B1 – B3 for “out-of-bag” set

Compound name	<i>CC</i> <sub>50</sub> class			<i>HNTC</i> class	
	Observed	Predicted (Model B1)	Predicted (Model B2)	Observed	Predicted (Model B3)
L-Val-Rim	1	0	1	1	1
L-Phe-Am	1	1	1	1	1
L-Phe(4-F)-Am	1	0	1	1	0
L-Val-Am	0	0	1	0	0
Gua-L-Val-Am	0	0	0	0	0
L-Tyr-Am	0	0	0	0	1
Gua-L-Tyr-Am	0	0	0	0	0
L-Gly-Rim	0	0	0	1	1
L-Ile-Rim	1	1	1	1	1
L-Leu-Rim	0	0	0	1	1
L-Phe-Rim	1	1	1	1	1
β-Ala-Rim	0	0	0	1	1
D-Phe(4-F)-Rim	1	1	1	1	1
Amantadine	0	0	0	0	0
Gua-L-β-Ala-Rim	0	0	0	0	0
L-Tyr-Rim	0	0	0	1	1
Gua-L-Tyr-Rim	0	0	0	1	1
L-Ala-Rim	0	0	0	1	1
Gua-L-Ala-Rim	0	0	0	0	0
L-Ala-Am	0	0	0	0	0
Gua-L-Ala-Am	0	0	0	0	0